PAPER

Check for updates

Solvent influenced synthesis of single-phase SnS$_2$ nanosheets for solution-processed photodiode fabrication†

D. Thangaraju, [iD] *[a] R. Marnadu,[b] V. Santhana,[a] A. Durairajan,[c] P. Kathirvel,[d] J. Chandrasekaran,[b] S. Jayakumar,[a] M. A. Valente[c] and Darius C. Greenidge[e]

The effect of variant high boiling point solvent combinations in the synthesis and photo-sensing characteristics of tin disulfide (SnS$_2$) thin nanosheets were investigated. Solvent dependent single-phase formation was observed by powder X-ray diffractometry (XRD), and results were verified with Raman spectroscopy measurements. Particles synthesized with only oleylamine show a mixed-phase, and two other solvent combinations such as oleylamine + oleic acid + n-octadecene, and oleylamine + oleic acid, show single-phase 2H–SnS$_2$, without phase contamination. Scanning and transmission electron microscopes were used to verify the orbicular and hexagonal shape of synthesized SnS$_2$ nanosheets. Well-characterized samples were employed to fabricate heterojunction photosensitive diodes using a p-type silicon substrate. Light-responsive measurement results of fabricated diodes indicate that the oleylamine + oleic acid synthesized sample show very high light-sensitivity, and the fill factor value of a fabricated diode is closer to the ideal diode.

1. Introduction

Reduced dimensionality in the materials offers a wide variety of technically beneficial optical, electronic, mechanical, and sensing properties.[1] Ultrathin two-dimensional metal dichalcogenides (2DMDs) with the stoichiometric formula of AB$_2$ (A = Mo, Sn, Nb, Ga, W; B = S, Se, Te), are technically valuable semiconducting materials that are broadly used in field-effect transistors, sensitive photodetectors, and photovoltaic devices.[2] The coating of 2D nanostructures on the semiconductor substrate requires highly sophisticated coating units under specialized conditions such as a high vacuum or an appropriate atmosphere for reducing contamination.[3] The main disadvantages of these coating technologies are high cost and the complexity of operation.[4] Solution-processed device fabrication is one of the more convenient methods followed by researchers, in order to reduce the fabrication cost, ease of fabrication, and complexity in material preparation.[5,6] Solution-processed thin film-making methods such as spin coating, doctor blading, roll to roll printing, drop-casting, and spray techniques can be used to prepare the uniform industrial-grade thin film, which can be used in solar cells and sensor device fabrication. The low temperature and ambient preparation environment used in this method allowed the opportunity for the use of a greater variety of materials and flexible substrates. Ultra-thin layers are possible with solution-processed methods for ultra-sensitive devices. The required size and single-phase nanostructured materials can be synthesized and utilized for particular device applications through this method.[5]

Tin disulfide (SnS$_2$) is an outstanding two dimensional n-type semiconducting material with the indirect bandgap of 2.18–2.42 eV.[7,8] Polytype structures are possible in SnS$_2$ materials such as 2H, 4H, 6H$_a$, 6H$_b$–SnS$_2$. The simplest 2H–SnS$_2$ polytype belongs to the hexagonal crystal system with $P\bar{3}m1$, which has three atoms in the unit cell extended to one sandwich layer.[9] The metal atoms of the materials are octahedrally co-ordinated to the chalcogen atom and form a triple S–Sn–S layer structure.[10] The stacked layers of the crystal structure of these materials interact with each other with weak Van der Waals forces, which allows the materials to form stable structures with few atomic layers. The highly earth-abundant, less complicated, low cost, and eco-friendly

[a] nano-crystal Design and Application Lab (n-DAL), Department of Physics, PSG Institute of Technology and Applied Research, Coimbatore-641062, Tamil Nadu, India. E-mail: dthangaraju@gmail.com; Tel: +91 8098768306
[b] Department of Physics, Sri Ramakrishna Mission Vidyalaya College of Arts and Science, Coimbatore 641 020, Tamil Nadu, India
[c] I3NAveiro, Department of Physics, University of Aveiro, 3810 193 Aveiro, Portugal
[d] Department of Physics, PSG College of Technology, Coimbatore-641004, Tamil Nadu, India
[e] Shizuoka University, Office of the Special Advisor to the President, International Affairs (Geologist/Mineralogist), 836, Ohya Suruga-ku, Shizuoka, 422-8529, Japan
† Electronic supplementary information (ESI) available. See DOI: 10.1039/c9ce01417a

Paper

nature of SnS$_2$, has helped to identify it as an emerging material for sustainable device applications.[11,12] Strong physical and chemical properties of this material enable it to be used as a potential candidate for batteries, as a photocatalyst, photodetector, in gas sensors, field emitters, and field-effect transistor (FET) applications.[13–17] Many methods are adopted to synthesize 2D single-phase SnS$_2$ nanostructures, such as wet chemical methods, hydrothermal, chemical vapor deposition, and chemical vapor transport methods.[18–21] Single-phase SnS$_2$ without Sn, SnS and Sn$_2$S$_3$ contamination and single poly-type were still a challenging process in a thin film preparation.

In this article, wet chemical synthesis was adopted to prepare SnS$_2$ nanostructures with different solvent combinations such as oleylamine (S0-SnS$_2$), oleylamine + oleic acid + n-octadecene (S1-SnS$_2$), oleylamine + oleic acid (S2-SnS$_2$). Possible single-phase SnS$_2$ formation using a high-temperature boiling point solvent combination, and the morphology-dependent photo response of SnS$_2$ in fabricated heterostructure photosensitive diodes were discussed in detail.

2. Experimental section

2.1. Materials

Tin(II) chloride (SnCl$_2$; 99.9%) and sulfur powder were purchased from Wako Pure Chemical Industries Ltd., Japan. High boiling point solvents like oleylamine (technical grade, 70%), oleic acid, and n-octadecene were procured from Sigma Aldrich. Cyclohexane and ethanol were used as purchased, from SRL chemicals. All the chemicals in this work were utilized as purchased, without any further purification.

2.2. Synthesis of single-phase SnS$_2$ nanoparticles

The high-temperature hot injection method was selected for the synthesis of SnS$_2$ nanosheets. For the synthesis of S0-SnS$_2$, one mmole of SnCl$_2$ precursor was mixed with oleylamine (5 mL) in a 100 mL three-necked flask (A). Similarly, two mmole sulfur powder was added with oleylamine (5 mL) in another 100 mL three-neck flask B. Both reaction flasks were heated to 140 °C, and the degassing process was performed in order to remove moisture from the solvent. The flask B was cooled to room temperature, and the sulfur dissolved clear solution was loaded into a glass syringe. In the meantime, flask A was heated to 250 °C, and the solution loaded syringe was injected into the flask with a nitrogen atmosphere. The final solution was kept at the same temperature for one hour and then cooled down to room temperature. The synthesized material was washed with ethanol, twice, and was stored in cyclohexane. In S1-SnS$_2$ synthesis, precursors like SnCl$_2$ (1 mmole) and sulfur powder (2 mmole) were dissolved in 1 mL oleylamine, 1.5 mL oleic acid, and a 3.5 ml n-octadecene combination separate three-neck flask, and the rest of the procedure is followed as mentioned above. 2.5 mL oleylamine and 2.5 mL oleic acid were used in S2-SnS$_2$ synthesis, as mentioned in the above procedures. Synthesized S0-SnS$_2$, S1-SnS$_2$, and S2-SnS$_2$

nanosheets were dispersed in a non-polar solvent like cyclohexane for thin-film formation.

2.3. Diode fabrication

Fig. 1 shows the schematic diagram of the heterojunction photosensitive device. The n-SnS$_2$/p-Si junction diodes were fabricated using S0-SnS$_2$, S1-SnS$_2$, and S2-SnS$_2$ on a 1 cm × 1 cm sized float zone p-Si substrate (100) plane. The Si substrate having ~260 (±30) μm thickness and ~40–50 (±5) Ω cm resistivity were used. The Si substrates were well cleaned using piranha solution (H$_2$O$_2$ + H$_2$SO$_4$) prepared by a 2 : 1 ratio to remove organic and metallic impurities. The Si substrates were soaked for 5 min in the HF + H$_2$O solution (1 : 10 in the ratio) to remove the SiO$_2$ layer from the substrate. All substrates were rinsed in de-ionized water while completing every step of the cleaning process. SnS$_2$ ink was prepared by dispersing as-synthesized SnS$_2$ (40 mg) in 1 ml of cyclohexane. Prepared SnS$_2$ ink was drop cast on the well cleaned p-Si substrate and was naturally dried in the natural ambiance for 20 min. The prepared devices were annealed at 320 °C under vacuum for one hour to remove surfactants on the SnS$_2$ nanosheets such as oleic acid and oleylamine. For I–V measurements, the high graded and low resistive silver past (ELTECK-corporation) was applied to the surfaces (both sides) of the device.

2.4. Instrumentation

The phase purity of as-synthesized nanosheets was found by 'X'PERT PANalytical powder X-ray diffraction (PXRD) with a scan rate of 2° min^{-1} in the 2θ range from 10° to 90°. A Jobin Yvon HR 800 Raman spectrometer was used for Raman spectral analysis of the as-synthesized samples under 532 nm excitation. The morphology change with the different solvent combinations was studied by an S-3400N Hitachi field emission scanning electron microscope (FESEM) and was verified by a high-resolution transmission electron microscopy (HRTEM) using a JEOL TEM 2100F microscope. The diode parameters of fabricated n-SnS$_2$/p-Si were measured by Keithley source meter (Model No.: 6517-B) under illumination with a xenon lamp (150 W short-arc) equipped portable solar simulator (PEC-L01).
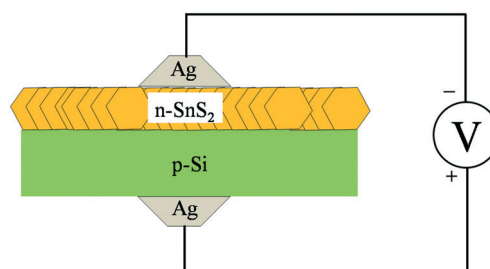

Fig. 1 Schematic diagram for n-SnS$_2$/p-Si diode.

3. Results and discussion

Acquired PXRD patterns of synthesized samples with three different solvent combinations are depicted in Fig. 2. High-intensity XRD reflections of S0-SnS$_2$ samples synthesized using oleylamine solvent showed that the particles were well matched with a hexagonal structure of 2H–SnS$_2$ (JCPDS card No.: 00-022-0951) and in addition to that, less intense peaks were observed, which matches with the orthorhombic structure of SnS (JCPDS card No: 00-014-0620). The XRD reflections of S1-SnS$_2$ and S2-SnS$_2$ samples showed that all the reflections were well matched with hexagonal 2H–SnS$_2$. There is no other phase like SnS, and another poly type SnS$_2$ appeared in S1-SnS$_2$ and S2-SnS$_2$, which confirms that the formed particles are in single-phase SnS$_2$.

Recorded Raman spectra of synthesized S0-SnS$_2$, S1-SnS$_2$, and S2-SnS$_2$ samples are compared in Fig. 3. Intense observed peaks were fitted with the two strong Raman active modes of 2H–SnS$_2$.[22] SnS$_2$ synthesized with oleylamine shows two extensive features of intense vibrational peaks at 166, 224, and 312 cm^{-1} which is assigned to the B$_{3g}$ mode of SnS, E$_g$ and A$_{1g}$ of SnS$_2$, respectively. The S1-SnS$_2$ sample showed one small broad feature and a sharp peak at 224 and 305 cm^{-1}. The A$_{1g}$ peak of the above sample was shifted towards lower cm^{-1}, which may be due to strain. One well-resolved peak at 314 cm^{-1} was observed for the S2-SnS$_2$ sample. The undetectable nature of the E$_g$ peak in S2-SnS$_2$ revealed that there is a reduction of scattering for in-plane scattering, which is evident for the ultra-thin nature of the sample.

SEM micrographs of S0-SnS$_2$, S1-SnS$_2$, and S2-SnS$_2$ samples are presented in Fig. 4. Images of S0-SnS$_2$ (Fig. 4(a–c)) showed sheet-like morphology with uneven edges. A orbicular clusters that appear as flattened lotus leaves were observed in the S1-SnS$_2$ sample; no sharp edges appeared. Hexagonally shaped, sheet-like morphology was observed in the S2-SnS$_2$ sample. This morphology is evidence that a small amount of
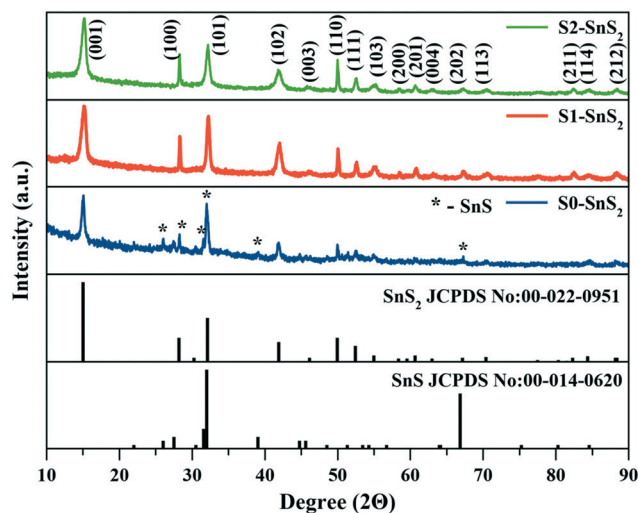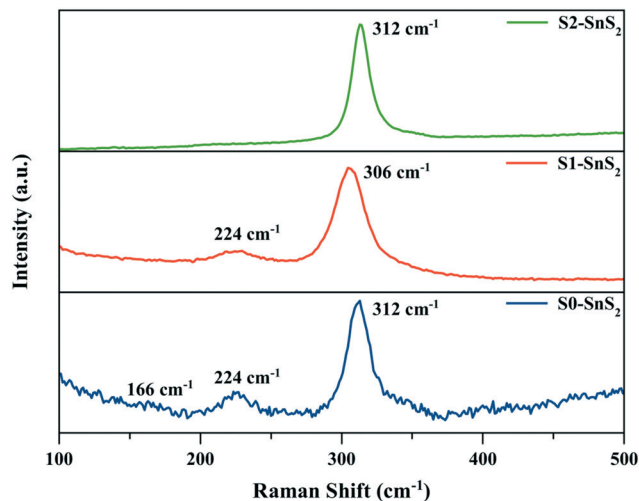

Fig. 3 Raman spectra of S0-SnS$_2$, S1-SnS$_2$, and S2-SnS$_2$ nanostructures.

n-octadecene addition changes the surface morphology and growth pattern at the edges in the S1-SnS$_2$.

TEM and HRTEM measurements revealed the particle formation and morphology of as-synthesized S0-SnS$_2$, S1-SnS$_2$, and S2-SnS$_2$ samples. TEM images of S0-SnS$_2$ revealed that there are two different natures of particles that are present in the sample, as shown in Fig. 5(a–f). A bulky particle with no proper shape was observed, along with tiny sphere-like particles. HRTEM lattice images showed evidence that the lattice distance (5.71 Å) of a bigger particle was matched with the (001) plane of SnS$_2$ and the lattice distance (3.46 Å) of the tiny sphere-like particles belonged to the (120) plane of SnS particles. The scattered TEM diffraction dot pattern also supports the formation of the mixed polycrystalline phase.

Fig. 6(a–f) shows the TEM, HRTEM, and SEAD pattern images of S1-SnS$_2$. A 2D sheet-like orbicular cluster was observed. Higher magnification images (Fig. 6d) revealed that the edge of the sheets is of indefinite shape and it appears as a lotus leaf-like shape with wavy like edges. HRTEM lattice images (Fig. 6e) give evidence of a lattice distance of 3.2 Å, which is perfectly matched with the (100) plane of SnS$_2$ material. Bright TEM diffraction dot patterns were recorded, as shown in Fig. 6f. Diffracted dots were identified as (100), (200), and (110) planes, which confirmed that the formed layer is the (001) plane layer of SnS$_2$. The growth of the SnS$_2$ sheets started at the center and extended outward with wavy patterned edges.

Hexagonal nanosheet-like morphology of the as-synthesized S2-SnS$_2$ sample was confirmed with TEM, HRTEM, and SAED patterns, as shown in Fig. 7(a–f). Hexagonal shape morphology with well-defined sharp edges was observed from TEM pictures. HRTEM images indicated the inter planer distance of 3.2 Å, which is associated with the (100) plane of SnS$_2$. Diffracted spots of the SAED pattern show evidence that the derived sheets were oriented along the (001) plane of SnS$_2$. The flat surface was recorded for S2-SnS$_2$, which supports the results of Raman analysis.
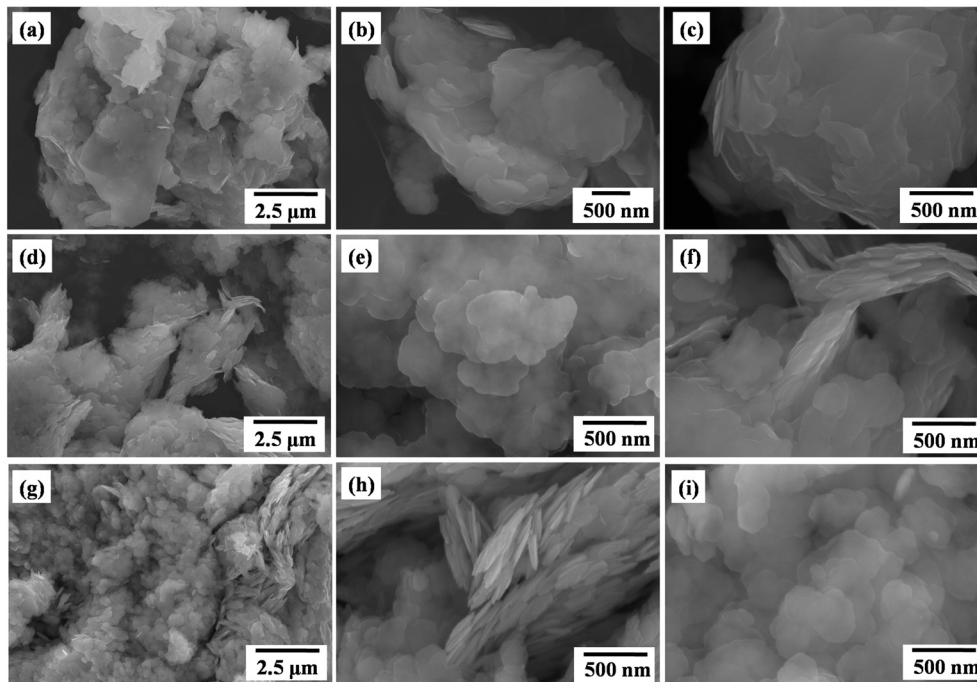

Fig. 2 Comparative XRD patterns of S0-SnS$_2$, S1-SnS$_2$, and S2-SnS$_2$ nanostructures.

Fig. 4 SEM micrographs of SnS$_2$ nanostructures synthesized using S0-SnS$_2$ (a–c), S1-SnS$_2$ (d–f) and S2-SnS$_2$ (g–i).
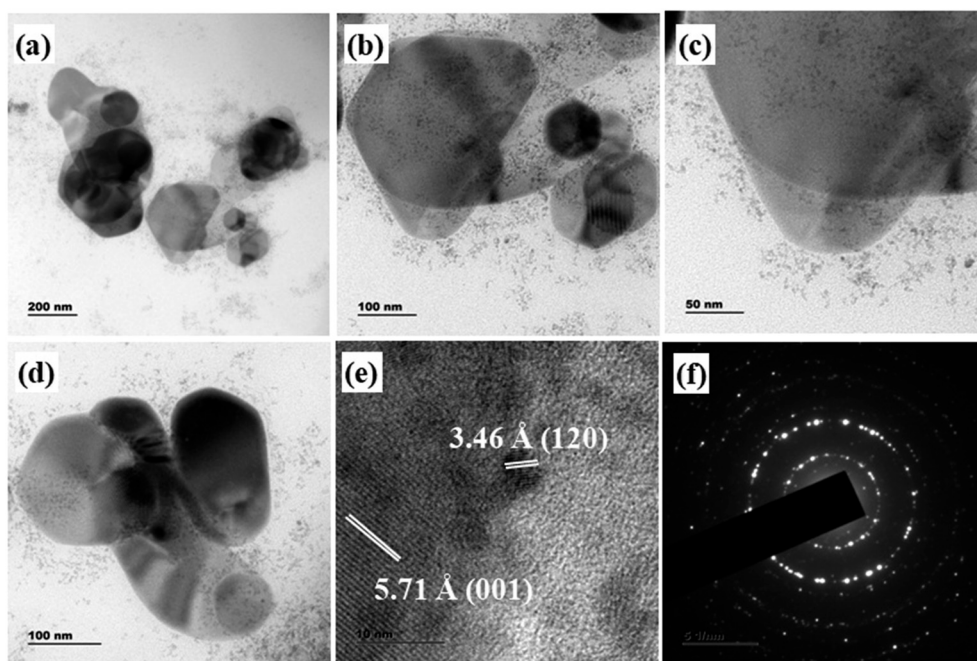

Fig. 5 TEM (a–d), HRTEM (e) and SAED pattern (f) images of S0-SnS$_2$ nanostructures.

The thickness of the individual nanosheets of the S2-SnS$_2$ sample is presented in Fig. 8 (a–c). HRTEM images confirmed that 12 layers of (001) plane atoms were combined and form a single sheet. The thickness of the obtained sheet was ~6 nm, and the flat surface was confirmed with this analysis. The surface of S1-SnS$_2$ is not flat when compared to the S2-SnS$_2$ samples (Fig. S1†).

The solvents like oleylamine and oleic acid are used as a surfactant as well as reducing agents. Among these, oleylamine acts as a solvent and also has high reduction capability. *n*-Octadecene is used as a solvent, which cannot be used as a surfactant. Previously reported results prove that oleylamine creates faster nucleation and faster growth of particles. At the same time, when it is mixed with oleic acid, the slower nucleation and slower growth of particles were
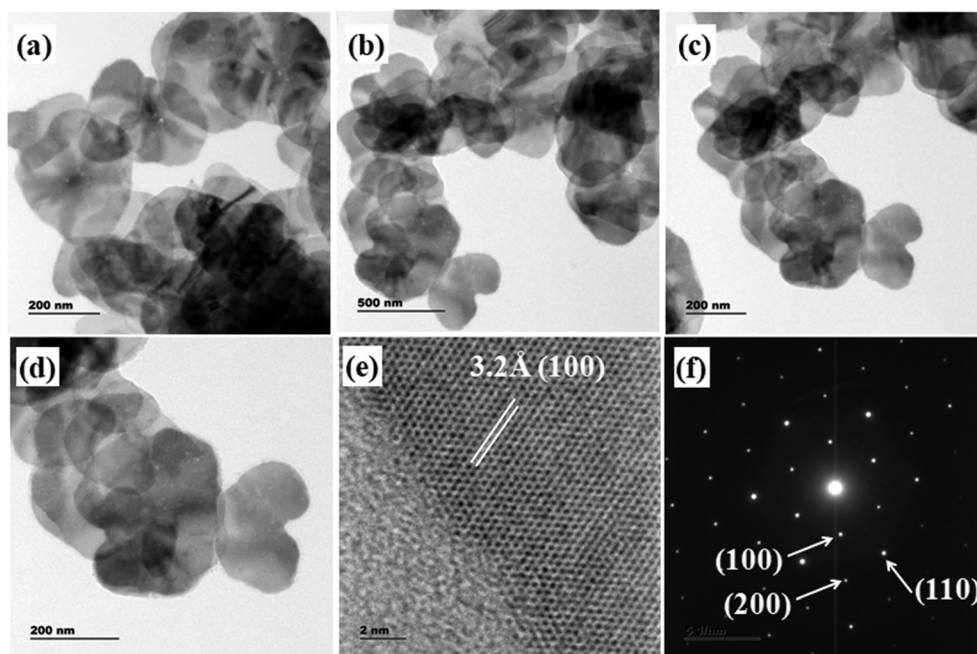
Fig. 6 TEM (a–d), HRTEM (e) and SAED pattern (f) images of S1-SnS$_2$ nanostructures.
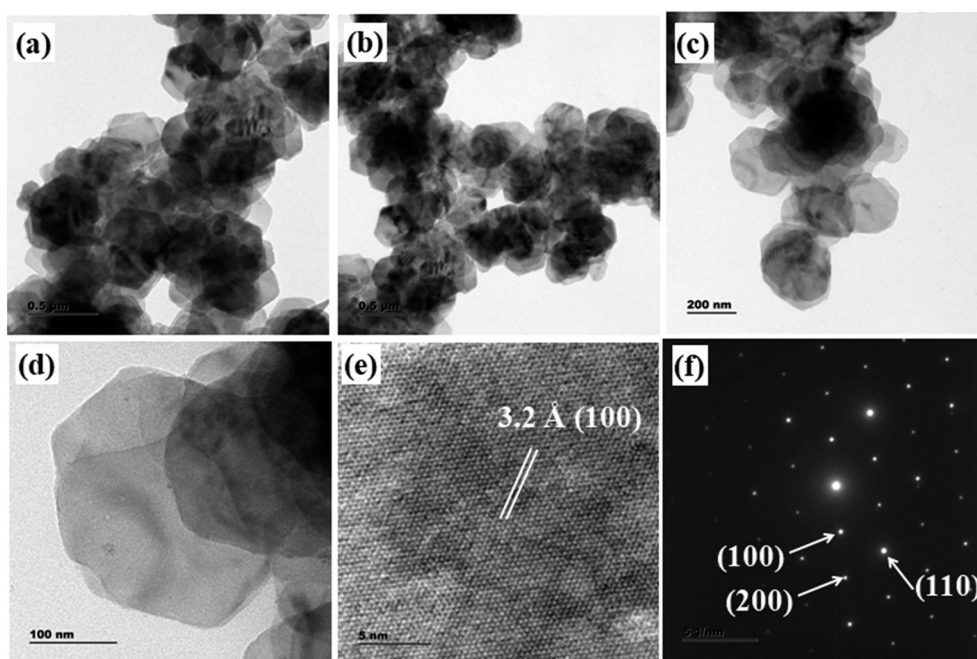

Fig. 7 TEM (a–d), HRTEM (e) and SAED pattern (f) images of S2-SnS$_2$ nanostructures.

observed.[23,24] The sample synthesized with oleylamine (S0-SnS$_2$) shows the presence of two phases in the sample, which reveals the formation of fast SnS and SnS$_2$ nucleation over a particular time. The flat and well-defined edge of S2-SnS$_2$ samples with the oleic acid and oleylamine combination may be due to slower nucleation and growth. Phase control was observed in S1-SnS$_2$, and the shape could not be controlled due to the dilution of the oleic acid and oleylamine combination with n-octadecene.

Photodiode parameters such as the ideality factor (n), barrier height (Φ_B), reverse saturation current (I_o), photosensitivity (P_S), responsivity (R), quantum efficiency (QE%), and specific detectivity (D^*) of the designed n-S0-SnS$_2$/p-Si, n-S1-SnS$_2$/p-Si, and n-S2-SnS$_2$/p-Si diodes were determined under dark and illumination field using a portable solar simulator (PEC-L01). The calculated photodiode parameters are summarized in Table 1. The forward and reverse current of all the diodes were assessed
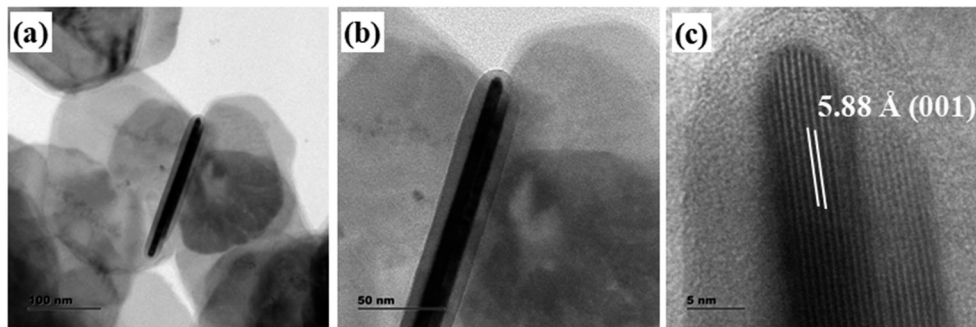
Fig. 8 TEM (a and b) and HRTEM (c) images of S2-SnS$_2$ nanostructures.

by applying bias voltage from −4 to +4 V using a Keithley electrometer (6517-B). The standard intensity of 1 sun (*i.e.*, 100 mW cm^{-2}) was fixed as measured intensity. Fig. 9 shows the I–V characteristics of the n-SnS$_2$/p-Si diodes fabricated with various solvents. It is worth mentioning here, that all the fabricated diodes show very fast photo-response under illumination conditions as shown in Fig. 9. Furthermore, the exponentially sharp increment of the current values to applied voltage and illumination also indicate the photo-conducting nature of n-SnS$_2$/p-Si diodes.[25] The calculated reverse saturation current (I_o) of the diodes was found to vary between 0.21 and 8.29 × 10^{-4} A.

The current flow through the n-SnS$_2$/p-Si diodes was explained by the thermionic emission theory model using the following equation.[26–29]

$$I = I_0 \left[\exp\left(\frac{q(V - IR_s)}{nK_B T}\right) - 1 \right] \tag{1}$$

Here,

$$I_0 = AA \times T^2 \exp\left(-\frac{q\phi_B}{K_B T}\right) \tag{2}$$

$$n = \frac{q}{K_B T}\left(\frac{d(V)}{d(\ln(I))}\right) \tag{3}$$

$$\Phi_B = \frac{K_B T}{q}\ln\left(\frac{AA \times T^2}{I_0}\right) \tag{4}$$

where q is the electron charge, V is the bias voltage, K_B is the Boltzmann constant, and T is the temperature.

The experimental value of n and Φ_B are the most critical parameters to analyze the devise performance, which were calculated from the eqn (3) and (4) using intercepts of semi-logarithmic plots of ln$J$ *vs.* voltage (V) as shown in Fig. 10. In general, the obtained n values are less than one, which indicates ideal behavior, and greater than one specifies the non-ideal in the nature of the diode. In the present study, the n-S2-SnS$_2$/p-Si diode exhibit lower n values (n = 3.33). This result might be attributed to the increment of photo-generated charge carrier under light conditions, swept of electrons and hole pairs, the conversion efficiency of Si and absorption of the n-type SnS$_2$ layer.[30–32]

Moreover, the obtained complete SnS$_2$ structure with 12 atomic layers of the prepared sample, may support the observed experiential n values, which have also been confirmed by XRD and TEM images. It is also observed that the n-S0-SnS$_2$/p-Si and n-S1-SnS$_2$/p-Si diodes exhibit higher n values, such as 13 and 12 under illumination, respectively. The existence of a thin oxide layer (SiO$_2$) among the n-SnS$_2$ layer and p-semiconductor junction may affect the barrier in-homogeneities. Also, the image-force effect, recombination of electron–hole pairs, and tunneling is the main reason for the diodes attaining higher n values.[33–36]

The barrier height of the diodes was changed from 0.639 to 0.734 eV. The diode Φ_B values are mostly affected by the interaction between the n-SnS$_2$ layer and Si surface along with the carrier tunneling traps and thickness of the n-type layer.[35] To compare the n-SnS$_2$/p-Si diode performance with a UV-photo-detector, we have calculated P_S, R, QE, and D^* of the diodes using the following the relations:[30]

$$P_s (\%) = \frac{I_{Ph} - I_D}{I_D} \times 100 \tag{5}$$

$$R = \frac{I_{Ph}}{PA} \tag{6}$$

$$EQE = \frac{Rhc}{q\lambda} \tag{7}$$

Table 1 Photodiode parameter n, Φ_B, I_o, P_S, R, QE% and D^* SnS$_2$/p-Si fabricated photodiode using S0-SnS$_2$ (a), S1-SnS$_2$ (b) and S2-SnS$_2$ (c) nanostructures

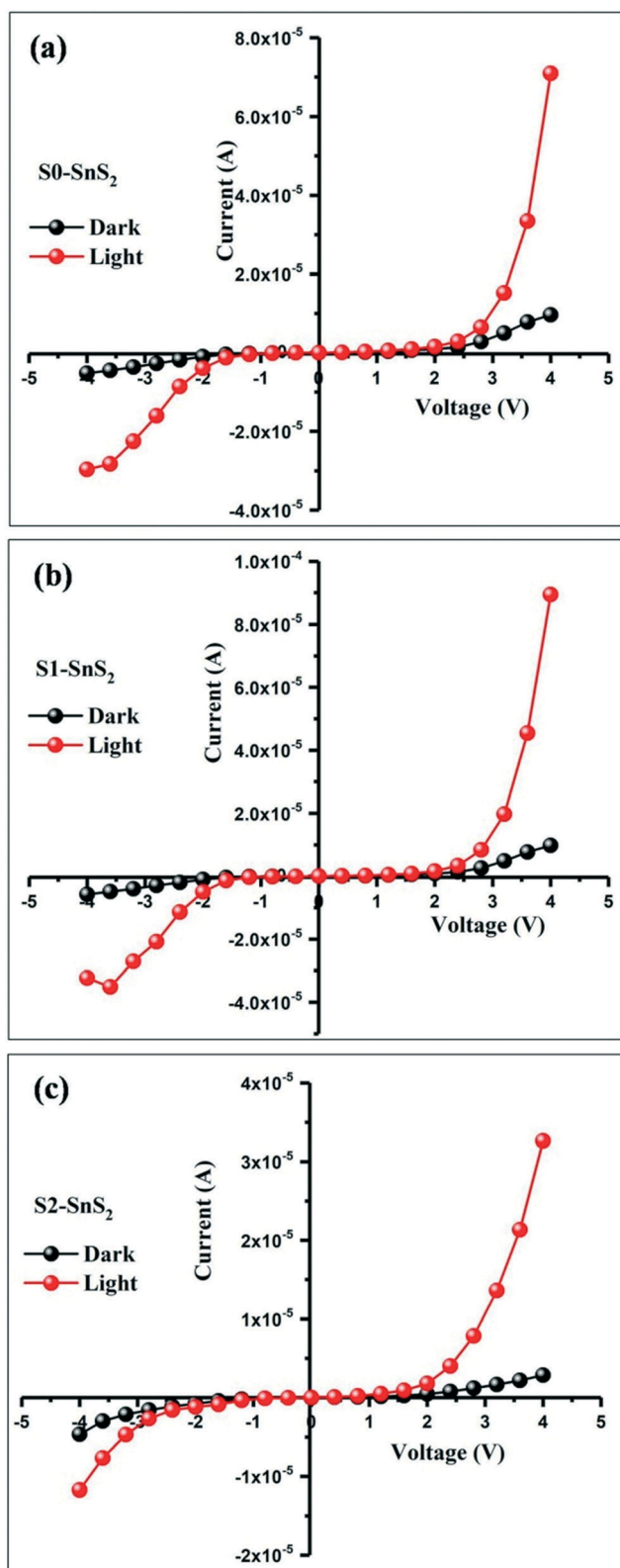| Diode	n		Φ_B (eV)		I_o (A)		P_S (%)	R (mA W^{-1})	QE (%)	D^* (×10^{10}) (Jones)
	Dark	Light	Dark	Light	Dark (×10^{-4})	Light (×10^{-4})				
n-S0-SnS$_2$/p-Si	12.56	13.09	0.651	0.639	5.24	8.29	637.87	44.33	17.19	2.5260
n-S1-SnS$_2$/p-Si	11.43	12.45	0.656	0.638	4.20	8.08	813.31	39.90	15.47	2.2533
n-S2-SnS$_2$/p-Si	6.90	3.33	0.692	0.734	1.07	0.21	1036.2	11.25	4.39	1.1813

Fig. 9 *I–V* characteristics of n-SnS$_2$/p-Si fabricated photodiode using S0-SnS$_2$ (a), S1-SnS$_2$ (b) and S2-SnS$_2$ (c) nanostructures.

Fig. 10 Semi-logarithmic plot of ln (*J*) *vs. V* for n-SnS$_2$/p-Si fabricated photodiode using S0-SnS$_2$ (a), S1-SnS$_2$ (b) and S2-SnS$_2$ (c) nanostructures.
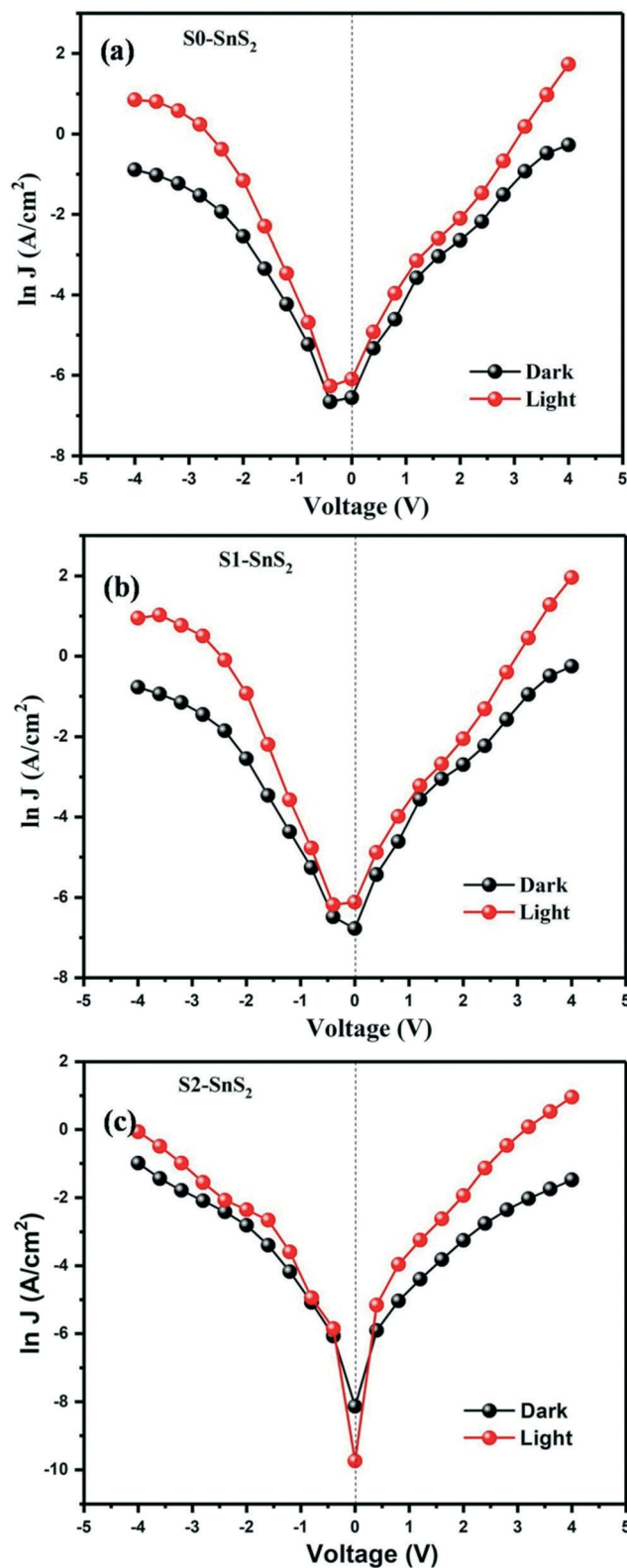
$$D^* = \frac{R}{(2qI_D)^{1/2}} \qquad (8)$$

where I_{Ph} is the photocurrent, I_D is the dark current, A is the area of the diode, P is the irradiation of the lamp, h is the

Planck's constant, c is the velocity of light, and λ is the wavelength. The calculated values of P_S, R, QE%, and D^* increase exponentially with increasing the applied voltage, as shown in Fig. 11. It is clear that the applied voltage strongly affected the photodiode parameters, particularly at a higher voltage. Remarkably, the n-S0-SnS$_2$/p-Si diode reached maximum photosensitivity of P_s (%) = 1036.2 at 4 V. This result suggests that the diode fabricated with oleylamine + oleic acid is highly sensitive under illumination. The photodiode with higher P_s (%) is more suitable for long-distance optical fiber communication systems.[37]

The calculated R was found to vary from 11.25 to 44.33 mA W^{-1}, which is in good agreement with reported values.[38–40] The variations in R is due to the surface oxygen adsorption–desorption process and surface to volume ratio of the SnS$_2$ layer.[41,42]

The external quantum efficiency is another important parameter to study the photodiode performance, which is directly proportional to the photon absorption coefficient of the device.[43] The maximum EQE of 17.19% was observed for the n-S0-SnS$_2$/p-Si diode at 4 V due to the increase in the light absorption at the depletion region. Specific D^* of the present diode was calculated from the bias voltage at 4 V using eqn (8). All the diodes show very high D^* = ~1–2 × 10^{10} Jones, which is a higher value than that of Zheng and Thambidurai et al.[44,45] From diode results, it is inferred that the n-S2-SnS$_2$/p-Si diode is very sensitive under illumination compared to other diodes.

The mixing of p-SnS in n-S0-SnS$_2$ samples affects the performance of n-S0-SnS$_2$/p-Si. Uneven surface and edges of S1-SnS$_2$ may be a reason for the poor performance, which may be due to more photon scattering and electron conduction problems. The better performance of the n-S2-SnS$_2$ may be due to the surface morphology and phase purity of the synthesized SnS$_2$ particles. The flat surface and defined edges of the nanosheets of S2-SnS$_2$ can form a layer by layer structure during the preparation of the thin film, which helps in the enhancement of its diode performance.

4. Conclusion

SnS$_2$ nanostructures were synthesized using three different high boiling point solvent combinations using oleylamine, oleic acid, and 1-ocatadecene. XRD patterns revealed that the samples synthesized using mixed solvents resulted in a single phase, which was confirmed by Raman analysis. SEM and TEM micrographs reveal the orbicular and hexagonal shape nanosheets of S1-SnS$_2$ and S2-SnS$_2$, respectively. The photodiode was successfully fabricated using as-synthesized SnS$_2$ nanosheets on a p-Si substrate. The ideality factor value of fabricated n-S2-SnS$_2$/p-Si photodiode is closer to an ideal diode, which can be employed in the fabrication of advanced sensing devices.

Conflicts of interest

There are no conflicts to declare.

Fig. 11 Comparison of photosensitivity, responsivity, quantum efficiency and specific detectivity *vs.* voltage graph of n-SnS$_2$/p-Si fabricated photodiode using S0-SnS$_2$ (a), S1-SnS$_2$ (b) and S2-SnS$_2$ (c) nanostructures.

References

1 G. Konstantatos, M. Badioli, L. Gaudreau, J. Osmond, M. Bernechea, F. P. G. De Arquer, F. Gatti and F. H. L. Koppens, *Nat. Nanotechnol.*, 2012, 7, 363–368.
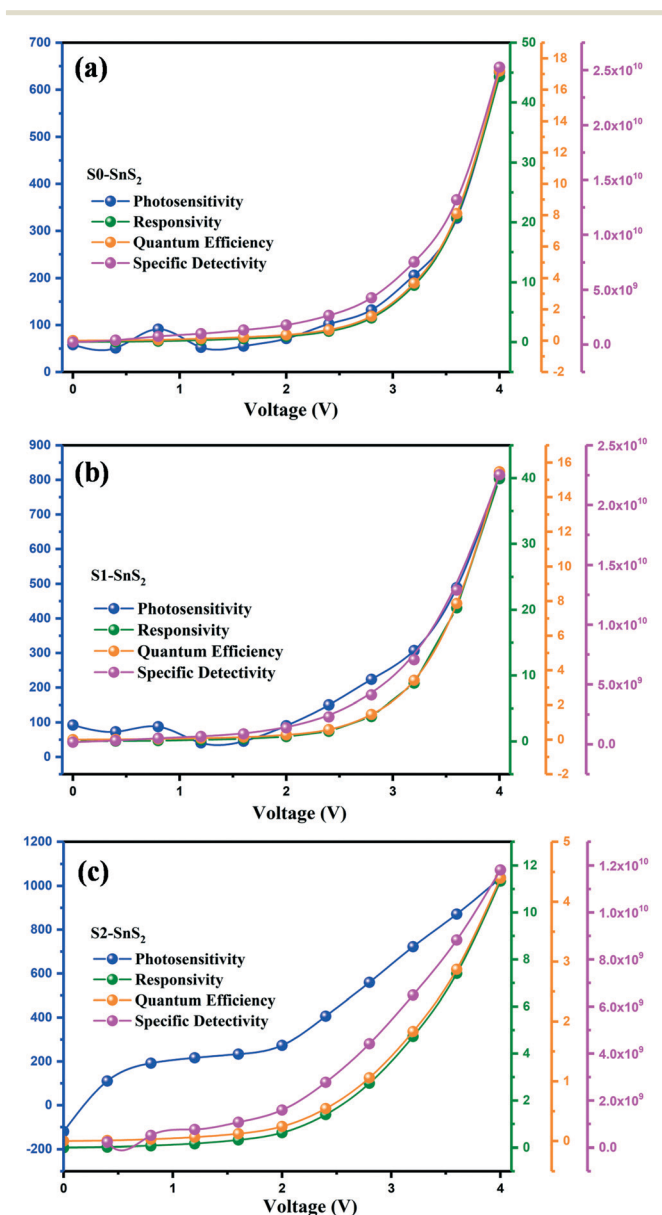
2 G. Yang, C. Zhu, D. Du, J. Zhu and Y. Lin, *Nanoscale*, 2015, **7**, 14217–14231.

3 F. P. García De Arquer, A. Armin, P. Meredith and E. H. Sargent, *Nat. Rev. Mater.*, 2017, **2**, 1–16.

4 C. C. Hsu, C. H. Chou, Y. T. Chen and W. C. Jhang, *IEEE Trans. Electron Devices*, 2019, **66**, 2631–2636.

5 X. Wang, W. Tian, M. Liao, Y. Bando and D. Golberg, *Chem. Soc. Rev.*, 2014, **43**, 1400–1422.

6 G. Sarasqueta, K. R. Choudhury and F. So, *Chem. Mater.*, 2010, **22**, 3496–3501.

7 H. B. Mabiala-Poaty, D. H. Douma, B. M'Passi-Mabiala and R. E. Mapasha, *J. Phys. Chem. Solids*, 2018, **120**, 211–217.

8 Y. Kumagai, L. A. Burton, A. Walsh and F. Oba, *Phys. Rev. Appl.*, 2016, **6**, 1–14.

9 Y. Huang, E. Sutter, J. T. Sadowski, M. Cotlet, O. L. A. Monti, D. A. Racke, M. R. Neupane, D. Wickramaratne, R. K. Lake, B. A. Parkinson and P. Sutter, *ACS Nano*, 2014, **8**, 10743–10755.

10 Y. Sun, H. Cheng, S. Gao, Z. Sun, Q. Liu, Q. Leu, F. Lei, T. Yao, J. He, S. Wei and Y. Xie, *Angew. Chemie - Int. Ed.*, 2012, **51**, 8727–8731.

11 J. Xia, G. Li, Y. Mao, Y. Li, P. Shen and L. Chen, *CrystEngComm*, 2012, **14**, 4279–4283.

12 W. Du, D. Deng, Z. Han, W. Xiao, C. Bian and X. Qian, *CrystEngComm*, 2011, **13**, 2071–2076.

13 M. Dragoman, M. Batiri, A. Dinescu, V. Ciobanu, E. Rusu, D. Dragoman and I. Tiginyanu, *J. Appl. Phys.*, 2018, **123**, 024506.

14 C. Fan, Y. Li, F. Lu, H. X. Deng, Z. Wei and J. Li, *RSC Adv.*, 2015, **6**, 422–427.

15 X. Zhou, Q. Zhang, L. Gan, H. Li and T. Zhai, *Adv. Funct. Mater.*, 2016, **26**, 4405–4413.

16 G. M. Kumar, F. Xiao, P. Ilanchezhiyan, S. Yuldashev and T. W. Kang, *RSC Adv.*, 2016, **6**, 99631–99637.

17 L. Sun, Z. Zhao, S. Li, Y. Su, L. Huang, N. Shao, F. Liu, Y. Bu, H. Zhang and Z. Zhang, *ACS Appl. Nano Mater.*, 2019, **2**, 2144–2151.

18 J. Yu, C. Y. Xu, F. X. Ma, S. P. Hu, Y. W. Zhang and L. Zhen, *ACS Appl. Mater. Interfaces*, 2014, **6**, 22370–22377.

19 C. Gurnani, S. L. Hawken, A. L. Hector, R. Huang, M. Jura, W. Levason, J. Perkins, G. Reid and G. B. G. Stenning, *Dalt. Trans.*, 2018, **47**, 2628–2637.

20 J. Z. Ou, W. Ge, B. Carey, T. Daeneke, A. Rotbart, W. Shan, Y. Wang, Z. Fu, A. F. Chrimes, W. Wlodarski, S. P. Russo, Y. X. Li and K. Kalantar-Zadeh, *ACS Nano*, 2015, **9**, 10313–10323.

21 G. Su, V. G. Hadjiev, P. E. Loya, J. Zhang, S. Lei, S. Maharjan, P. Dong, P. M. Ajayan, J. Lou and H. Peng, *Nano Lett.*, 2015, **15**, 506–513.

22 A. J. Smith, P. E. Meek and W. Y. Liang, *J. Phys. C: Solid State Phys.*, 1977, **10**, 1321–1333.

23 X. Yin, M. Shi, J. Wu, Y. Pan, D. L. Gray and H. Yang, *Nano Lett.*, 2017, **17**, 6146–6150.

24 X. Yin, M. Shi, K. S. Kwok, H. Zhao, D. L. Gray, J. A. Bertke and H. Yang, *Nano Res.*, 2018, **11**, 3442–3452.

25 M. Balaji, J. Chandrasekaran, M. Raja and R. Marnadu, *Mater. Res. Express*, 2019, **6**, 106404.

26 V. Balasubramani, J. Chandrasekaran, R. Marnadu, P. Vivek, S. Maruthamuthu and S. Rajesh, *J. Inorg. Organomet. Polym. Mater.*, 2019, **29**, 1533–1547.

27 R. Marnadu, J. Chandrasekaran, M. Raja, M. Balaji, S. Maruthamuthu and P. Balraju, *Superlattices Microstruct.*, 2018, **119**, 134–149.

28 P. Vivek, J. Chandrasekaran, R. Marnadu, S. Maruthamuthu and V. Balasubramani, *Superlattices Microstruct.*, 2019, **133**, 106197.

29 R. Marnadu, J. Chandrasekaran, P. Vivek, V. Balasubramani and S. Maruthamuthu, *Zeitschrift fur Phys. Chemie*, 2019, DOI: 10.1515/zpch-2018-1289.

30 R. Marnadu, J. Chandrasekaran, S. Maruthamuthu, V. Balasubramani, P. Vivek and R. Suresh, *Appl. Surf. Sci.*, 2019, **480**, 308–322.

31 R. Marnadu, J. Chandrasekaran, M. Raja, M. Balaji and V. Balasubramani, *J. Mater. Sci.: Mater. Electron.*, 2018, **29**, 2618–2627.

32 I. Arsel, M. Turmus, O. Pakma, C. Ozaydin and O. Gullu, *J. non oxide Glas.*, 2017, **9**, 33–46.

33 S. Alialy, S. Altindal, E. E. Tanrikulu and D. E. Yildiz, *J. Appl. Phys.*, 2014, **116**, 083709.

34 Ş. Altindal, H. Kanbur, D. E. Yildiz and M. Parlak, *Appl. Surf. Sci.*, 2007, **253**, 5056–5061.

35 H. K. Khanfar, A. F. Qasrawi, Y. A. Zakarneh and N. M. Gasanly, *IEEE Sens. J.*, 2017, **17**, 4429–4434.

36 S. Karatas, S. Altindal, A. Turut and M. Cakar, *Phys. B*, 2007, **392**, 43–50.

37 B. Prasanna Lakshmi, V. Rajagopal Reddy, V. Janardhanam, M. Siva Pratap Reddy and J. H. Lee, *Appl. Phys. A: Mater. Sci. Process.*, 2013, **113**, 713–722.

38 Q. L. Tan, W. D. Zhang, C. Y. Xue, J. J. Xiong, J. H. Li, T. Liang and Y. B. Shi, *2008 2nd IEEE Int. Nanoelectron. Conf. INEC 2008*, 2008, vol. 8, pp. 776–781.

39 J. Yao and G. Yang, *Small*, 2018, **14**, 2–9.

40 D. Shao, M. Yu, J. Lian and S. Sawyer, *Nanotechnology*, 2013, **24**, 295701.

41 Y. Zhang, T. Ji, W. Zhang, G. Guan, Q. Ren, K. Xu, X. Huang, R. Zou and J. Hu, *J. Mater. Chem. C*, 2017, **5**, 12520–12528.

42 P. A. Shaikh, D. Shi, J. R. D. Retamal, A. D. Sheikh, M. A. Haque, C. F. Kang, J. H. He, O. M. Bakr and T. Wu, *J. Mater. Chem. C*, 2016, **4**, 8304–8312.

43 A. A. Ahmed, M. Devarajan and N. Afzal, *Surf. Rev. Lett.*, 2017, **24**, 1750096.

44 Z. Zheng, J. Yao and G. Yang, *ACS Appl. Mater. Interfaces*, 2017, **9**, 14920–14928.

45 M. Thambidurai, Y. Jang, A. Shapiro, G. Yuan, H. Xiaonan, Y. Xuechao, Q. J. Wang, E. Lifshitz, H. V. Demir and C. Dang, *Opt. Mater. Express*, 2017, **7**, 2326.